Supplementary Information (SI) for Journal of Materials Chemistry A.

Electronic Supporting Information (ESI)

Hydration-Driven Enhancement of Interstitialcy Oxide-Ion Diffusion

Yuichi Sakuda,[a] Mudasir A. Yatoo,[b] Bhuvaneshwari Manivannan,[c] Vediyappan Veeramani,[c] Junko Habasaki,[a] Stephen J. Skinner,[b,c] Hiroshige Matsumoto[c,d] & Masatomo Yashima[a,d] *

a Department of Chemistry, School of Science, Institute of Science Tokyo, 2-12-1 W4-17 Ookayama, Meguro-ku, Tokyo 152-8551, Japan.

b Department of Materials, Imperial College London, London, SW7 2AZ, UK.

c International Institute for Carbon-Neutral Energy Research (WPI-I2CNER), Kyushu University, 744 Motooka, Nishi-ku, Fukuoka 819-0395, Japan.

d Center for Energy Systems Design (CESD), International Institute for Carbon Neutral Energy Research (WPI-I2CNER), Kyushu University, 744 Motooka, Nishiku, Fukuoka 819-0395, Japan.

* Corresponding author: yashima.m.5864@m.isct.ac.jp

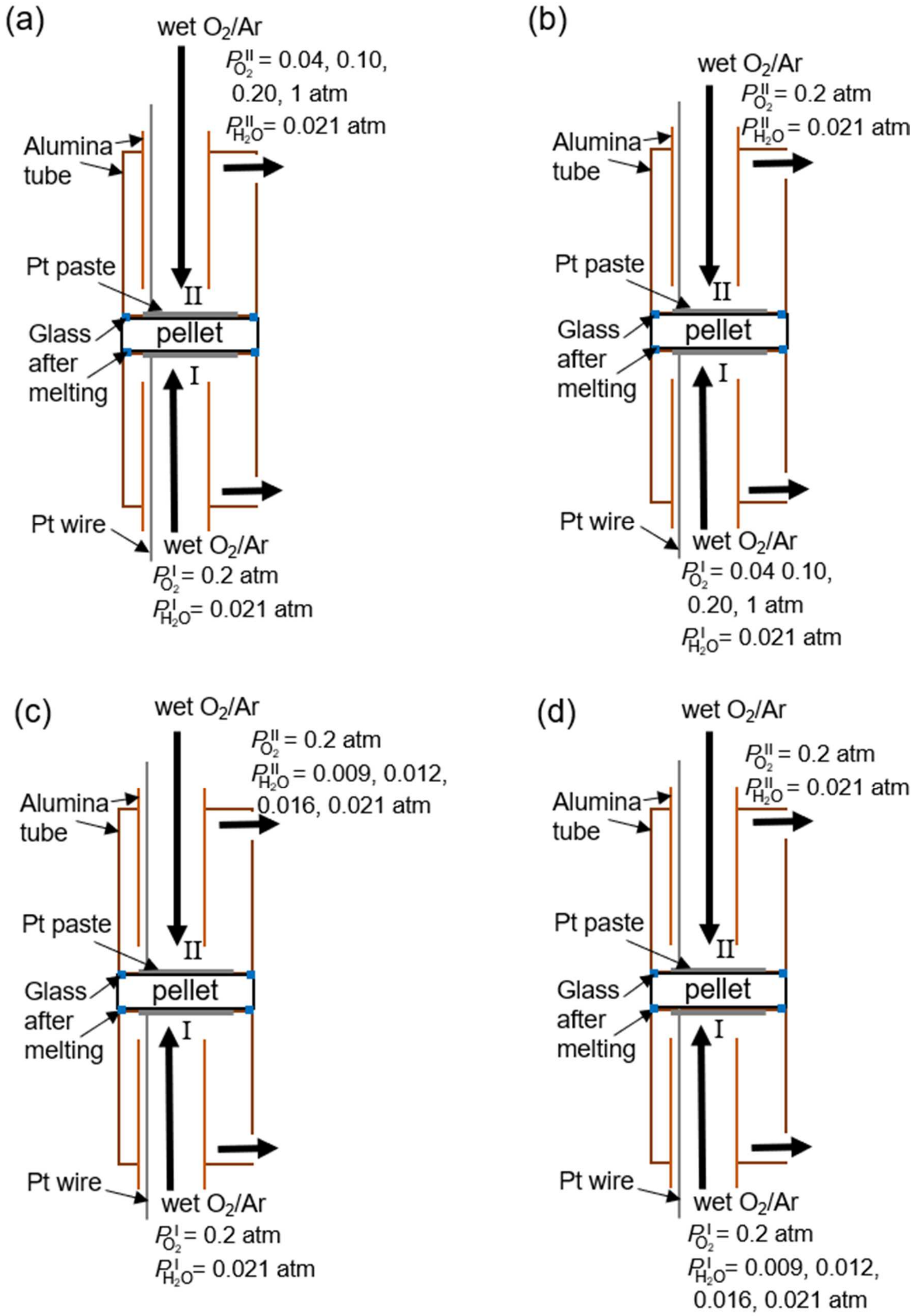

Figure S1. Schematics of (a,b) the oxygen and (c,d) water vapor concentration cells for EMF measurements at 500 and 600 °C. The pellet stands for the $Ba_7Nb_4MoO_{20}$ sample.

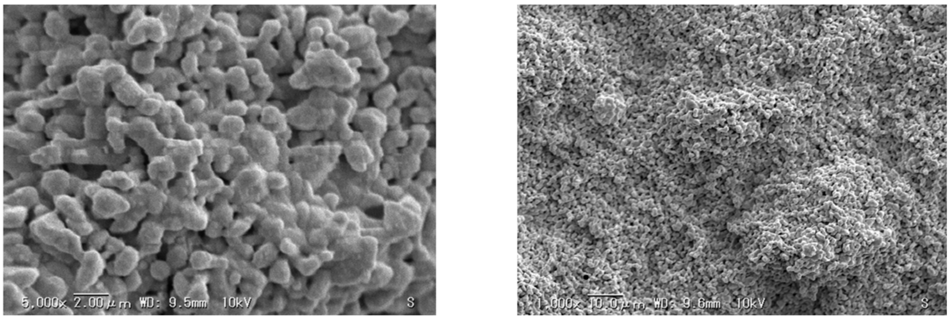

Figure S2. SEM images of a sintered $Ba_7Nb_4MoO_{20}$ pellet, which was polished and thermally etched at 1150 ºC for 2 hours prior to the SEM observation. The average grain was 1.8 μm.

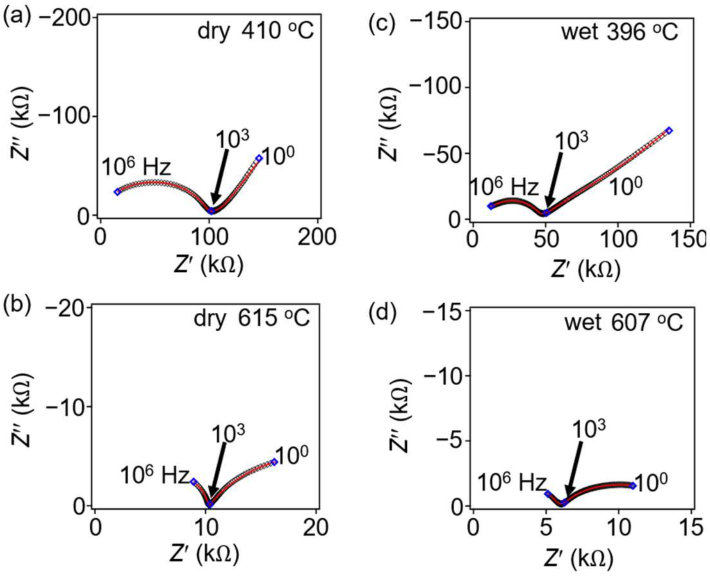

Figure S3. Complex impedance plane plots of $Ba_7Nb_4MoO_{20}$ at (a) 410 and (b) 615 °C in dry air and at (a) 396 and (b) 607 °C in wet air (pH_2O = 0.021 atm). Black rhombuses and red lines represent measured data and equivalent circuit fittings, respectively.

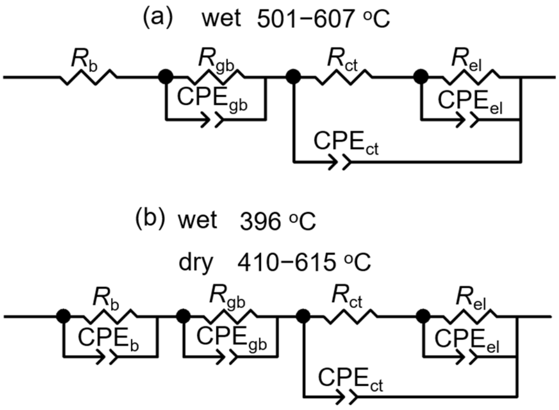

Figure S4. Equivalent circuits used to model the impedance spectra of $Ba_7Nb_4MoO_{20}$ (a) from 501 ºC to 607 ºC in wet air and (b) from 410 ºC to 615 ºC in dry air and at 607 ºC in wet air. *R* and CPE denote a resistor and a constant phase element, respectively. The subscripts b, gb, el and ct represent bulk, grain boundary, electrode and charge transfer, respectively. The bulk and grain boundary capacitances were 0.9–11 pF and 0.01–0.02 nF, suggesting the bulk and grain boundary responses, respectively.

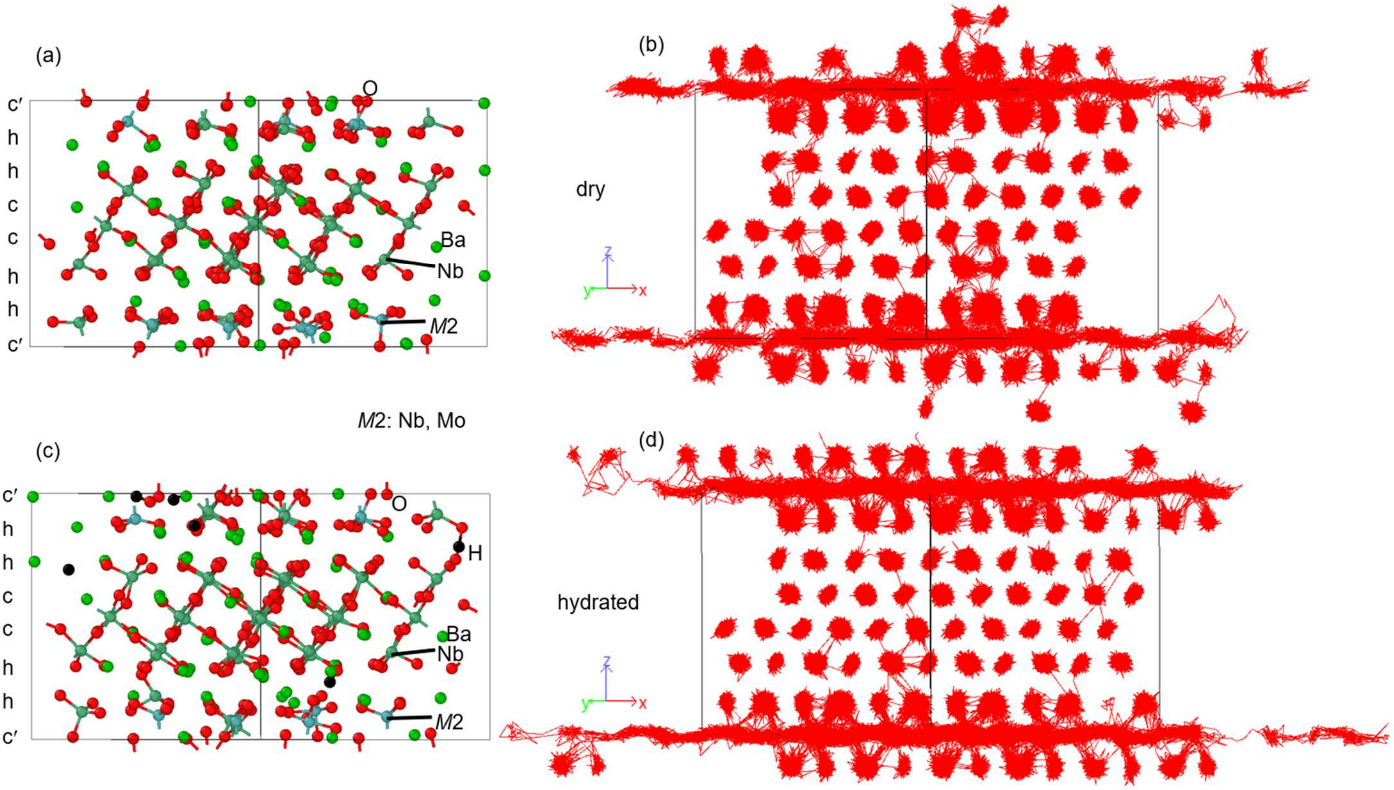

Figure S5. (a,c) Atomic arrangements of (a) dry and (c) hydrated $Ba_7Nb_4MoO_{20}$ at 0 ps in MSD at 1200 K (Fig. S6 for (a) and Fig. 7c for (c)), showing the layered structure consisting of hexagonal close packed BaO_3 h layers, cubic close packed BaO_3 c layers, and oxygen-deficient cubic close packed (BaO_2 for (a) and $BaO_{7/3}$ for (c)) c′ layer. (b,d) Trajectories of oxygen atoms of (b) dry and (d) hydrated $Ba_7Nb_4MoO_{20}$ at 1200 K. The atomic arrangements and trajectories were obtained by M3GNet-MD simulations.

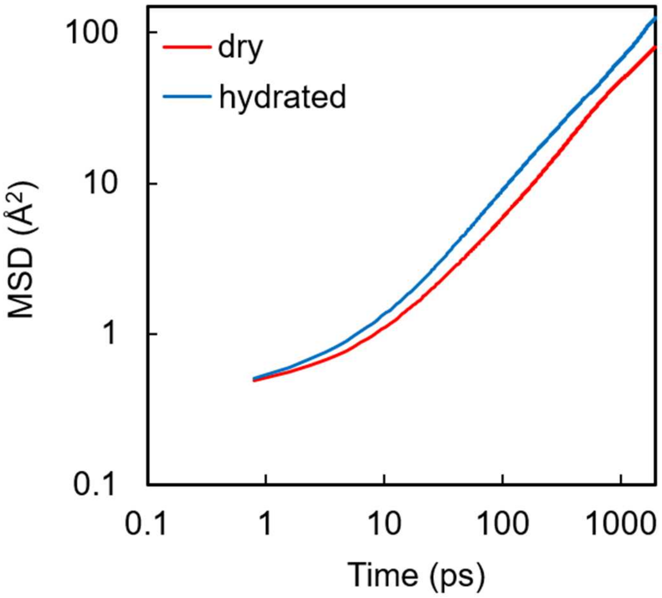

Figure S6. Mean-square displacement (MSD) of oxide ions versus time in log-log scale of dry $Ba_7Nb_4MoO_{20}$ (red line) and hydrated $Ba_7Nb_4MoO_{20}$ (blue line) at 1200 K.

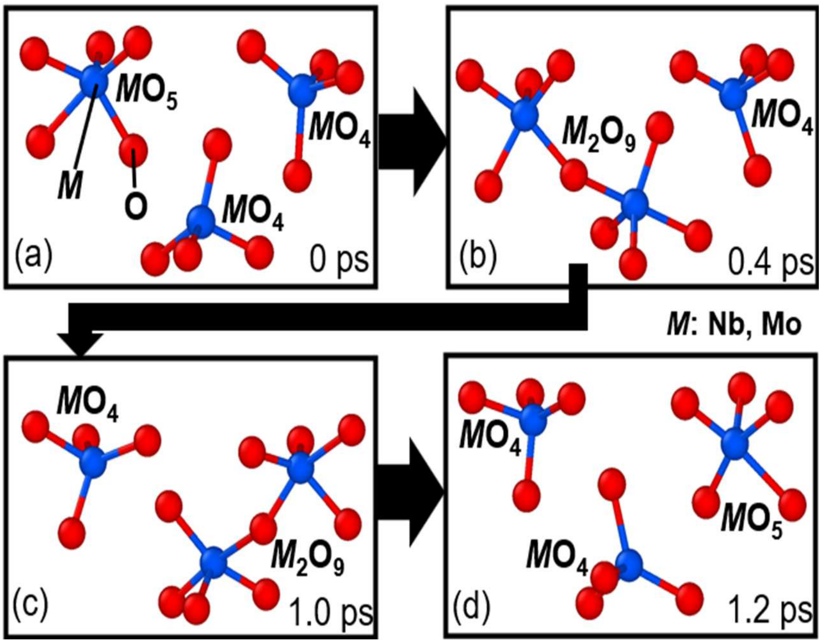

Figure S7. Snapshots of oxygen diffusion process of dry $Ba_7Nb_4MoO_{20}$ at 1200 K. The blue spheres (*M*) represent Nb or Mo cation. The red spheres (O) denote oxide ions. The time was set to 0 ps for the state of (a).

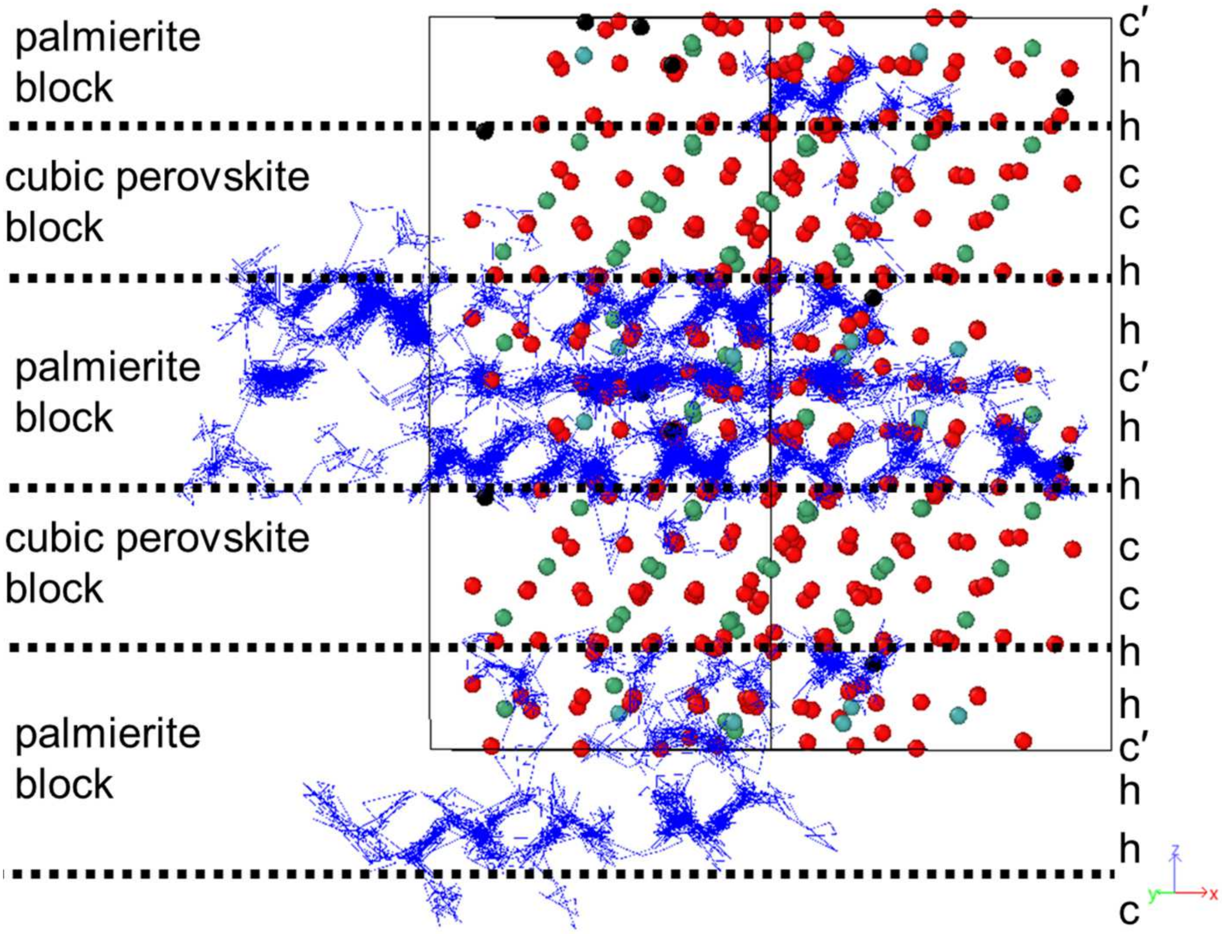

Figure S8. Trajectories of protons of hydrated $Ba_7Nb_4MoO_{20}$ at 1200 K, which were obtained by M3GNet-MD simulations. Protons show long-range migration in the palmierite blocks. Protons mainly migrate in the hexagonal close-packed (hcp) h layer, although they also migrate in the oxygen-deficient cubic close-packed (ccp) c′ layer.

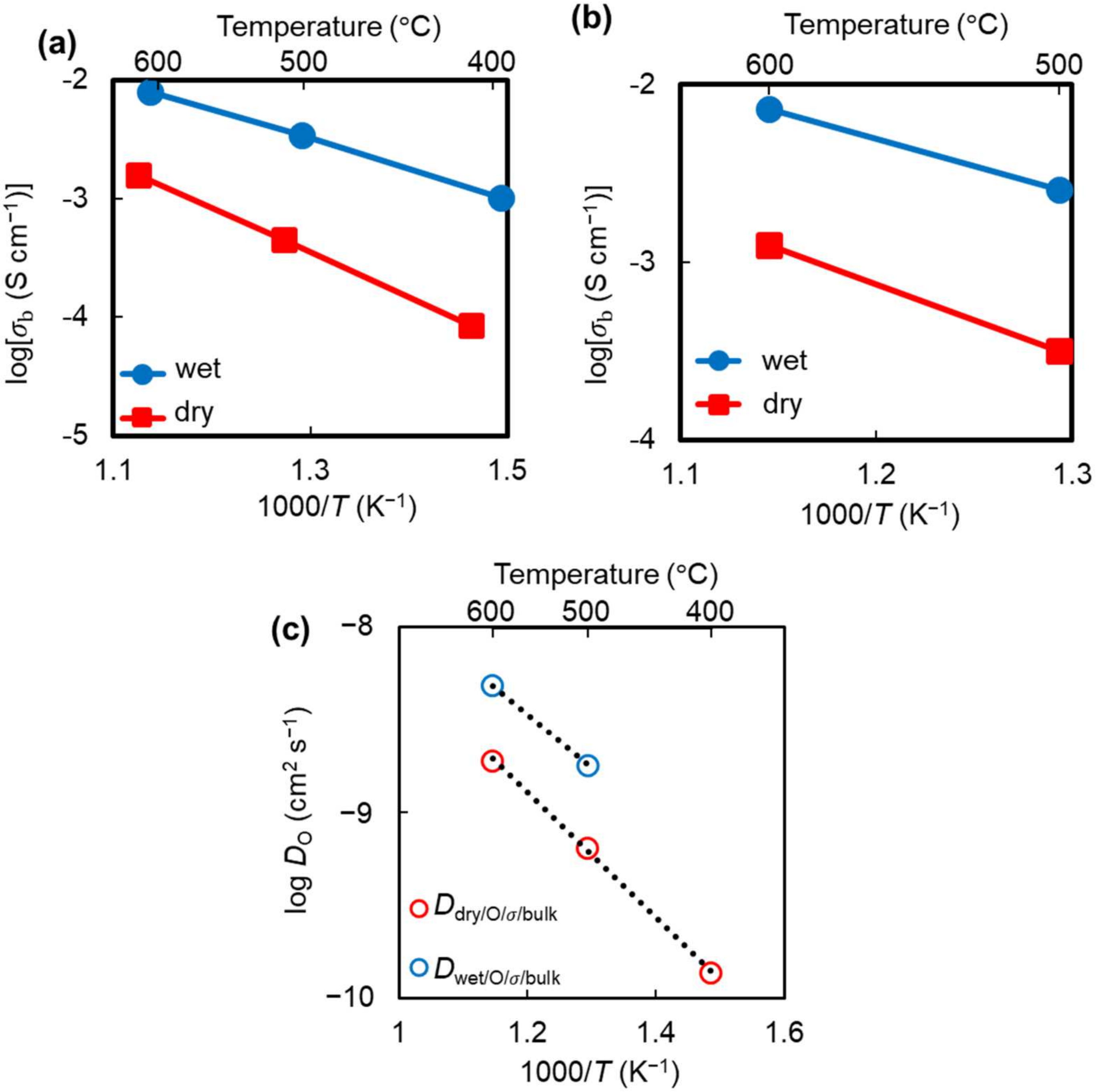

Figure S9. (a) Arrhenius plots of the bulk conductivity σ_b of $Ba_7Nb_4MoO_{20}$ in wet air (pH_2O = 0.021 atm; blue closed circles and line) and dry air (red closed squares and line). (b) Arrhenius plots of the bulk oxide-ion conductivity σ_b of $Ba_7Nb_4MoO_{20}$ in wet air (pH_2O = 0.021 atm; blue closed circles and line) and dry air (red closed squares and line). (c) Arrhenius plots of the bulk oxygen diffusion coefficients D_O of $Ba_7Nb_4MoO_{20}$ in wet air (pH_2O = 0.021 atm; blue open circles and black dotted line) and dry air (red open circles and black dotted line).

Supplementary Note: Bulk Conductivity, Apparent Transport Number, Bulk Oxide-Ion Conductivity, and Bulk Oxygen Diffusion Coefficient.

Equivalent circuit analyses were performed to extract the bulk conductivity (Fig. S4). Fig. S9a shows the Arrhenius plots of the bulk conductivities for $Ba_7Nb_4MoO_{20}$ in wet air $\sigma_{\mathrm{wet/bulk}}$ and in dry air $\sigma_{\mathrm{dry/bulk}}$. The $\sigma_{\mathrm{wet/bulk}}$ was higher than $\sigma_{\mathrm{dry/bulk}}$ at each temperature, which is consistent with the literature.[S1] The apparent oxygen transport number $t_{\mathrm{O/app/bulk}}$ was calculated from the bulk conductivities by the following simple equation (S1):

$$t_{\mathrm{O/app/bulk}} = \frac{\sigma_{\mathrm{dry/bulk}}}{\sigma_{\mathrm{wet/bulk}}} \qquad \text{(S1).}$$

The apparent oxygen transport number $t_{\mathrm{O/app/bulk}}$ (= 0.07–0.16) was low. The apparent proton transport number $t_{\mathrm{H/app/bulk}}$ was estimated from the bulk conductivities using the following equation (S2).

$$t_{\mathrm{H/app/bulk}} = \frac{\sigma_{\mathrm{wet/bulk}} - \sigma_{\mathrm{dry/bulk}}}{\sigma_{\mathrm{wet/bulk}}} \qquad \text{(S2)}$$

The $t_{\mathrm{H/app/bulk}}$ values (= 0.93–0.84) were large, which was consistent with the literature.[S1] At first glance, it appears that protons are the main conducting species in bulk $Ba_7Nb_4MoO_{20}$ in wet atmospheres. However, this is not the case as shown by the accurate transport number measurements using the oxygen and water vapor concentration cells. Indeed, the accurate transport number of oxide ions 0.955-0.76 is much higher than that of protons 0.045-0.24 (Fig. 3a,b in the main text). The oxide-ion conductivities in wet and dry atmospheres were calculated using the following equations (S3) and (S4):

$$\sigma_{\mathrm{wet/O/EMF/bulk}} = \sigma_{\mathrm{wet/bulk}} \times t_{\mathrm{wet/O/EMF}} \qquad \text{(S3)}$$

$$\sigma_{\mathrm{dry/O/EMF/bulk}} = \sigma_{\mathrm{dry/bulk}} \times t_{\mathrm{dry/O/EMF}} \qquad \text{(S4)}$$

Here, $t_{\mathrm{dry/O/EMF}}$ (~1) is the oxygen transport number estimated by EMF measurements with an oxygen concentration cell in dry atmospheres reported in the literature.[S1] The bulk oxide-ion conductivity in wet atmosphere $\sigma_{\mathrm{wet/O/EMF/bulk}}$ was higher than that in dry condition $\sigma_{\mathrm{dry/O/EMF/bulk}}$ (Fig. S9b; $\sigma_{\mathrm{wet/O/EMF/bulk}} > \sigma_{\mathrm{dry/O/EMF/bulk}}$), indicating the enhancement of bulk oxide-ion conductivity. We estimated the carrier concentration (number of oxide ions per volume) and oxygen diffusion coefficient using the bulk oxide-ion conductivity and Nernst-Einstein equation:

$$D_{\mathrm{dry/O/\sigma/bulk}} = kT\sigma_{\mathrm{dry/O/EMF/bulk}}/(4e^2 n_{\mathrm{dry/O}})$$

$$D_{\mathrm{wet/O/\sigma/bulk}} = kT\sigma_{\mathrm{wet/O/EMF/bulk}}/(4e^2 n_{\mathrm{wet/O}}).$$

Here, k is the Boltzmann constant, T is the absolute temperature, e is the elementary charge, $n_{\mathrm{dry/O}}$ is the number of oxide ions per volume in dry conditions, $n_{\mathrm{wet/O}}$ is the number of oxide ions per volume in wet atmospheres. The Haven ratio is assumed to be unity. As shown in Fig. S9c, the bulk oxygen diffusion coefficient in wet atmospheres $D_{\mathrm{wet/O/}\sigma\mathrm{/bulk}}$ was significantly higher than that in dry condition $D_{\mathrm{dry/O/}\sigma\mathrm{/bulk}}$ ($D_{\mathrm{wet/O/}\sigma\mathrm{/bulk}} > D_{\mathrm{dry/O/}\sigma\mathrm{/bulk}}$), indicating the enhancement of bulk oxygen diffusivity by hydration, which is consistent with the MSDs of oxygen atoms obtained by the M3GNet-MD simulations. The reason for the higher bulk conductivity in wet atmosphere than that in dry condition is the enhancement of bulk oxide-ion conductivity by hydration, which is attributed to the enhancement of bulk oxide-ion diffusivity by hydration.

Supplementary Reference

S1. S. Fop, K. S. McCombie, E. J. Wildman, J. M. S. Skakle, J. T. S. Irvine, P. A. Connor, C. Savaniu, C. Ritter and A. C. Mclaughlin, *Nat. Mater.*, 2020, **19**, 752.